Applied Problems of Nonlinear Oscillation and Wave Theory

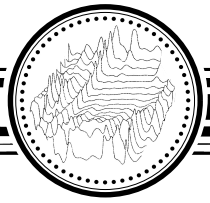

Article DOI: 10.18500/0869-6632-003145

Influence of Gaussian noise and Levy noise on the phase dynamics of the ensemble of Kuramoto-like oscillators of first- and second-order

Arinushkin P. A.[1]✉, *Kupriyanov V. D.*[2], *Vadivasova T. E.*[2]

[1]TatITneft LLC Artificial Intelligence Competence Center, Almetyevsk, Russia
[2]Saratov State University, Russia
E-mail: ✉arinushkin.pavel@gmail.com, kuprijn@mail.ru, vadivasovate@yandex.ru
Received 6.08.2024, accepted 18.09.2024, available online 2.12.2024, published 30.05.2025

Abstract. The *purpose* of this study is to determine the stability threshold of the dynamic modes of the ensemble of phase Kuramoto-like oscillators, describing the behavior of a simple power grid model with a ring topology, under the external influence of Gaussian noise and Levy noise. The results are evaluated to determine the threshold values of noise at which the considered dynamic model is the most sensitive to noise and demonstrates a change of the steady state. *Methods.* In this paper, two ensembles of Kuramoto-like phase oscillators with the same topology but different numbers of oscillators are investigated. The ensembles consist of first-order and second-order phase oscillators modeling the dynamics of generators and consumers in the power grid, respectively. In this work, maps of the regimes are computed and used, from which regions with different synchronous dynamics are selected. In the selected regions, a set of initial conditions is fixed and the ensemble under study is modeled in the presence of noise of different types and intensities. The obtained result is evaluated with the help of calculated spatio-temporal diagrams, values of the Kuramoto parameter, and statistical characteristics estimated from the realizations of oscillations in time. *Results.* It is shown that a power grid model consisting of Kuramoto-like phase oscillators exhibits different robustness to external noise disturbances depending on the type of noise disturbance and the steady-state dynamic regime. It was demonstrated that the frequency synchronization mode of all oscillators, independent of the initial conditions, is insensitive to the influence of white noise of high intensity, both Gaussian and Levy noise. In the region of coexistence of coexistence of synchronous and asynchronous behavior, depending on the initial conditions, a change in phase dynamics under the influence of different noise is observed. The numerical experiment shows that the power grid model is more susceptible to Levy noise due to the noise features associated with random bursts, which in turn can be interpreted as random impulses. *Conclusion.* In a power grid model represented by two ensembles consisting of different numbers of Kuramoto-like phase oscillators of first-order and second-order, different modes of frequency and phase dynamics of the oscillators are established. A numerical experiment with the influence of Gaussian noise and Levy noise is carried out for the obtained modes. It is shown that the model under study is more sensitive to Levy noise, the influence of which leads to a change of the dynamic mode due to strong random pulses.

Keywords: power grids, phase oscillators, Kuramoto oscillators, nonlinear coupling, phase synchronization, noise effects, Gaussian noise, Levy noise.

Acknowledgements. This work was supported by the Russian Science Foundation (project No. 20-12-00119).

For citation: Arinushkin PA, Kupriyanov VD, Vadivasova TE. Influence of Gaussian noise and Levy noise on the phase dynamics of the ensemble of Kuramoto-like oscillators of first and second order. Izvestiya VUZ. Applied Nonlinear Dynamics. 2025;33(3):289–306. DOI: 10.18500/0869-6632-003145

Introduction

One of the priorities in the field of numerical modeling of physical processes is to consider the dynamics of power systems of various types and complexity. The development of urban infrastructure fully depends on the technological development of power grids. A particularly important factor in the operation of any power grid is the resilience to external influences and the geographical availability of electricity.

The problem of geographical availability of electricity sources lies in the impossibility of building a power station in a given area due to the peculiarities of the terrain features, which, in turn, entails the use of power stations located far from energy consumers. In this case, the power grid becomes more centralized, which may affect its resistance to external influences, such as cascading power grid failures or transmission line failures. Renewable energy sources are used as a solution to the problem of electricity availability. This approach makes it possible to reduce the load on a centralized power station or completely phase it out. However, the inclusion of such elements in the power grid has difficulties related to synchronization and normal operation [1–9]. One of the considered tasks of this study is related to solving the problems of global sustainability and synchronization of power grids. Solutions to these problems are found both from the standpoint of technical improvement of power grids and through mathematical modeling. Of particular interest among scientists is the study of the effects and phenomena of synchronization of power grids, as this approach makes it possible to approach the solution of the problem associated with the sustainable behavior of power stations.

The dynamics of the power grid are well described using coupled nonlinear oscillators [10–21]. Different models of nonlinear oscillators serve as different approximations to the real behavior of power grids. For example, the Kuramoto phase oscillator model allows us to simplifies the analysis of stability and synchronization of power grids [22, 23]; however, this model does not take into account the role and influence of inertia of electric generators, which is present in the dynamics of non-renewable power stations and in traditional sources of electricity. To account for inertia, the rotator model, that is, the model of phase oscillators with inertia [24–28]. Our work uses a combined power grid model taken from the article [24]. A special feature of this model is that generators are described taking into account inertia, that is, as rotators, and consumers as Kuramoto phase oscillators without inertia. This approach allows us to take into account the dynamics of not only energy generators but also consumers.

Despite the growth of renewable sources and the general decentralization of power grids, the main problem continues to be the frequency synchronization of power generators in the event of malfunctions and external influences disrupting the behavior of the network. The main types of external influences in the power grid are noise and pulse effects. Interference in an electrical network can be classified as background noise, which varies over long periods of time, and impulsive disturbances, which are short-lived. Background noise, in turn, can be divided into colored noise, which is mainly created by household electronic equipment such as computers, dimmers, or hair dryers [29], and narrowband fluctuations caused by radio broadcasting and power emissions. Connecting or disconnecting electronic devices can cause aperiodic pulse interference of the network frequency. In other cases, due to the rectifiers included in the power supply, periodic pulse interference may occur in the network, synchronous with the main frequency or with a frequency of repetition of interference multiples of 50/60 Hz. The network also has asynchronous periodic pulse noise with a repetition rate of 50-200 kHz [29–35]. According to [36–38], interference in the electrical network can be represented as the sum of the previously mentioned types of impacts. The presented papers [39–43] demonstrate that photovoltaic inverters, battery chargers, energy-efficient lighting, hydropower systems, wind turbines, or chargers for

electric vehicles, among other objects, are the main sources of high-amplitude conductive fluctuations. Other devices, such as motors [40], lighting devices [44,45] or electronic amplifiers, produce high-amplitude noise emissions with a wide range of spectral characteristics. The key goal of power grid research is to identify the mechanisms for the sustainable operation of power grids and their smooth functioning.

The purpose of this study is to consider a power grid with a ring topology and homogeneous parameters, modeled by an ensemble of interacting rotators and first-order phase oscillators [24] in the presence of noise sources such as Gaussian noise and Levy noise, to identify the threshold of stability of the power grid when various noise characteristics change, and to evaluate changes in spatial and temporal structures in a model of a power grid with dynamic consumers under the effect of various noise characteristics.

1. The investigated model and methods of numerical research

1.1. Power grid parameters and coupling architecture. The power grid under study consists of two types of elements; these are generators and consumers of electricity, which are connected via transmission lines. The presented elements and transmission lines have a wide range of characteristics to describe the operation of the power grid. Based on the methodology presented in the article [24], the initial stage of calculating the power grid is to define a set of physical quantities (Table 1).

Table 1. Power grid characteristics

Characteristics of generators							Characteristics of consumers		
x_i'	H_i	D_i	$P_{g(\text{active}),i}$	$P_{g(\text{reactive}),i}$	ω_R	$V_{g,i}$	$P_{c(\text{active}),i}$	$P_{c(\text{reactive}),l}$	$V_{c,l}$
0.0608	$4.4c$	50	2	0	314.15 rad/s	1.04	2	0	1.04

Here H_i is the inertia parameter of the generator, D_i is the dissipation parameter, x_i' is the transient reactance of the rotor and stator windings of the generator. Each generator is characterized by the values of the active $P_{g(\text{active}),i}$ and reactive power $P_{g(\text{reactive}),i}$, whereas for energy consumers these parameters specify the consumption of active $P_{c(\text{active}),l}, l = 1, ..., n_c$, and reactive power $P_{c(\text{reactive}),l}, l = 1, ..., n_c$, respectively. The output voltages of generators and consumers are designated as $V_{g,i}$ and $V_{c,i}$ respectively. The reference frequency of the power grid $\omega_R = 314.15$ rad/s (50 Hz). The parameter indexes take the values $i = 1, 2, 3..., n_g$ and $l = 1, 2, 3..., n_c$ for generators and consumers, respectively, where n_g is the total number of generators and n_c is the total number of consumers. Parameters x_i', H_i, D_i, $P_{g(\text{active}),i}$, $P_{g(\text{reactive}),i}$, $V_{g,i}$ are selected to be identical for all generators, and parameters $P_{c(\text{active}),l}$, $P_{c(\text{reactive}),l}$, $V_{c,l}$ are selected to be identical for consumers. It is also worth noting that the presented power and voltage parameters are dimensionless quantities, with power normalized to 100 MW and voltage to 100 kV.

The transmission line of the power grid (Table 2) has the same set of values of physical quantities. Depending on the type of connection, these values are individual. The transmission line is represented as a π-model in which the active resistance r is connected to the inductive element x in series. Two capacitances equal to b are connected in parallel to the series connection of the resistance and inductance, which form a P-link with all elements. The values of the elements in the π-model are normalized to values of 1 Ohm/m for active resistances, for inductors at 1 H/m, and for capacitances at 1 F/m. The parameter τ is the voltage transformation coefficient, and ψ is the phase shift of the voltage. According to the methodology proposed in [24], the generator is divided into two elements: the generating part and the external generator node,

Table 2. Transmission line characteristics

Connection type	r	x	b	τ	ψ
generator — external generator node	0	0.0576	0	1	0
external generator node — consumer	0.0085	0.072	0.149	1	0

which have a purely inductive coupling between each other, as shown in Table 2. The studied topology is a ring of alternating elements of generators and consumers. Such a coupling between the elements is presented in the connection type «external generator node — consumer» in Table 2.

The grid characteristics presented in Tables 1 and 2 are used by the MATPOWER program [46] to calculate the power grid admittance matrix $\mathbf{Y}$. This matrix is used to calculate the right parts of the phase oscillator equations. In turn, the parameters of the right-hand of equations (1) and (4) are calculated in the program provided by the authors of the article [24]. The data presented in Tables 1 and 2 are based on test data from the New England power supply system with 10 generators, the characteristics of which are described in the article [47]. We carried out changes to the test data of the initial power supply system, selecting the average values for each presented element of the power grid in order to obtain an idealized power grid in which the physical parameters of the network elements were homogeneous and the power grid itself represented a simple ring topology. The purpose of this approach is to consider the phase dynamics of a complex model of phase equations presented in [24] using simpler examples of power grids.

1.2. Kuramoto-like phase oscillators of first and second order. The studied model of a power grid with dynamic consumers [24] is represented in the form of Kuramoto-like phase oscillators of the first and second order. The equation for a power grid generator is represented as a phase oscillator with inertia or a rotator and is written as

$$\frac{2H_i}{\omega_R}\ddot{\delta}_i + \frac{D_i}{\omega_R}\dot{\delta}_i = A_i^g - K_{i,i+n_g}^g \sin(\delta_i - \delta_{i+n_g}) + \sigma\xi_i(t), \quad i = 1, \cdots, n_g, \tag{1}$$

$$A_i^g = P_{g(\text{active}),i}, \tag{2}$$

$$K_{i,i+n_g}^g = |E_i V_i / x_i^{'}|. \tag{3}$$

For consumers, the equation of the model looks like the equation of a first-order phase oscillator:

$$\frac{D_l}{\omega_R}\dot{\delta}_l = A_l - \sum_{j=n_c, j\neq l}^{N} K_{lj}\sin(\delta_l - \delta_j - \gamma_{lj}) + \sigma\xi_l(t), \quad l = n_c, \cdots, N, \tag{4}$$

$$A_l = -P_{c(\text{active}),l} - |V_l|^2 G_{ll}, \tag{5}$$

$$K_{lj} = |V_l V_j Y_{lj}|, \tag{6}$$

$$\gamma_{lj} = \alpha_{lj} - \frac{\pi}{2}, \tag{7}$$

$$\mathbf{Y} = |Y_{lj}| e^{j\alpha_{lj}}, \quad \mathbf{j} = \sqrt{-1}, \tag{8}$$

$$|E_i|^2 = \left(\frac{P_{g(\text{active}),i} x_i'}{|V_i|}\right)^2 + \left(|V_i| + \frac{P_{g(\text{reactive}),i} x_i'}{|V_i|}\right)^2, \tag{9}$$

The parameters and variables in the equations are defined as follows: ω_R is the reference angular frequency of the system (in rad/s); $\dot{\delta}_i$ is the instantaneous rotation frequency of the i-th

oscillator relative to ω_R; H_i (in seconds) and D_i are inertia parameters and the dissipation of the i-th generator, respectively. The parameters A_i^g and A_i in equations (2) and (5) represent the dimensionless capacity parameters of the generator and consumer, respectively, taking into account dissipative losses. $P_{g(\text{active}),i}$ is the dimensionless active generated power of the generator, $P_{c(\text{active}),l}$ is the dimensionless active power of the consumer, $|E_i|$ and V_i are the dimensionless voltages of the generator and the consumer (including the output nodes of the generators). $\mathbf{G}$ is the real part of the dimensionless admittance matrix $\mathbf{Y}$. The parameter K_{ij} in equation (6) defines the coupling strength between oscillators numbered i and j, expressed as the product of the dimensionless voltages V_i, V_j of two coupled generating nodes and the complex admittance matrix $\mathbf{Y}$ between them. In the case of the coupling strength of the generator (equation (3)) the parameter $K^g_{i,i+n_g}$ is expressed in terms of the ratio of the product of the dimensionless voltage of the generator E_i and the dimensionless voltage of the output node of the generator V_i to the transient reactance $x_i^{'}$. The parameter γ_{ij} in equation (7) characterizes the phase shift in the coupling chain. The additive noise in the studied model is introduced into all the oscillators of the ensemble and is represented by independent normalized sources $\xi_i(t)$ for generators and $\xi_l(t)$ for consumers. The parameter σ sets the noise intensity. The dimensionless matrix $\mathbf{Y}$, obtained from the characteristics of the studied power grid, is used to compute the parameters A_i, A_i^g, K_{ij}, $K^g_{i,i+n_g}$, γ_{ij} in the right-hand sides of equations (1), (4) and is the conduction matrix of the elements of the network. The calculated parameter matrices of the right part of the equation for the studied power grid have the following dimensions: $\mathbf{A^g}(1\times n_g)$, $\mathbf{A}(1\times n_c)$, $\mathbf{K^g}(n_g\times n_g)$, $\mathbf{K}(n_c\times n_c)$, $\gamma(n_c\times n_c)$.

In this paper, we will use two ensembles modeling the power grid, described by equations (1)–(9) but with different numbers of elements. The first ensemble of the power grid consists of $N = 40$ elements, of which 10 are generators, 10 are the output nodes of generators, 10 are consumers with zero active and reactive power consumption and 10 are consumers with non-zero active and reactive power consumption. The output nodes of the generators are connected to consumers with zero active and reactive power. Consumer nodes with zero active and reactive power, in turn, are connected to ordinary consumers, forming a ring topology. The second ensemble of the power grid includes $N = 30$ network elements, of which 10 are generators, 10 are the output nodes of generators, and 10 are consumers. In this case, the output nodes of the generators are connected to ordinary consumers, forming a ring topology. In the presented ensembles of power grids, generators will be described by the differential equation (1), while the rest of the network elements, such as the output nodes of generators and various consumers, will be described by the differential equation (4).

2. Research results

The study of the phase dynamics of two power grids under various noise effects is divided into two tasks. In the first task, a regime map is calculated for the phase and frequency dynamics of the model and the obtained regimes are analyzed. The second task is to study the various noise effects on the obtained regimes in order to determine the threshold values of the intensities of various types of noise and assess the sensitivity of the model to external influences. The presented regime maps were obtained by integrating the system of equations (1)–(9) by the Heun's method of the 2nd order with an integration step of $h = 0.01$ on the dimensionless time of the system $T = 11000$. At the same time, integration at the time of setting the first 1000 units was not taken into account to eliminate the transition process in the model. All the presented regime maps were obtained using 50 different random normally distributed initial conditions.

2.1. Analysis of phase and frequency dynamics in ensembles of phase oscillators of different sizes. To conduct a numerical experiment with the noise effect on the power grid, we will perform a numerical calculation of the frequency and phase maps of the regimes for the two studied ensembles of phase oscillators. All the mode maps given in the article were constructed for a random spread of initial conditions, where the initial values of the variables are normally distributed quantities with zero mean and variances $d_{\dot{\delta}}$ and d_{δ} of the distributions for instantaneous frequencies and phases of the oscillators, respectively. In Fig. 1 *(a, d)* the regimes based on the calculation of the average frequencies of the oscillators (1) and (4) are presented. The phase synchronization regions for ensembles of 30 and 40 oscillators are identical and have almost identical boundaries. On the presented maps, you can see that the spread of the initial phases of the oscillators significantly affects the phase synchronization. Thus, with the value of the variance of the initial phases $d_{\delta} \approx 0.8$ there is a wide area of coexistence of synchronous and asynchronous dynamics. Synchronous or asynchronous behavior depends on the initial conditions. It is also worth noting that the phase synchronization mode is always observed in region 1, regardless of the initial conditions. In Fig. 1 *(b, c, e, f)* maps of the values of the Kuramoto order parameter [48] is presented. The order parameter characterizes the degree of phase coherence of the ensemble's oscillators and is calculated using the formula

$$r(t)e^{i\chi(t)} = \frac{1}{n}\sum_{j=1}^{N} e^{i\theta_j(t)}, \tag{10}$$

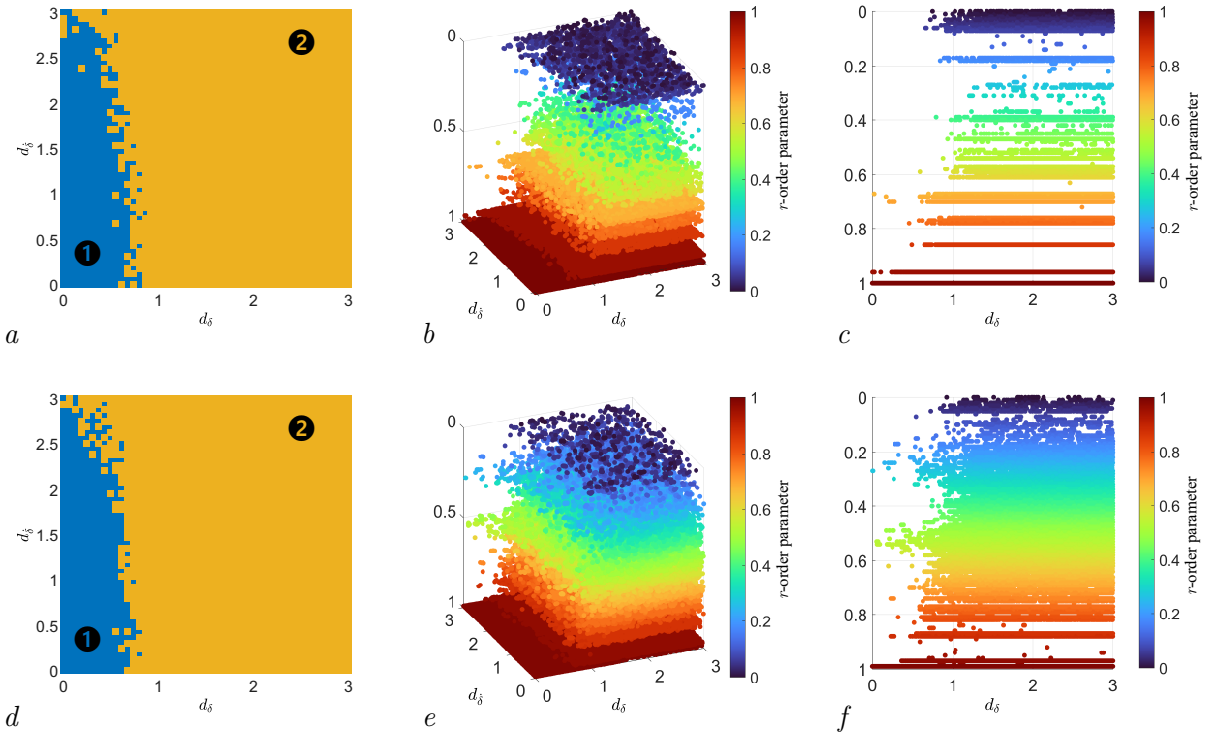

Fig. 1. Maps of ensemble modes depending on the variance of initial phase values and instantaneous frequencies: *a, d* — by the mean value and variance of oscillator frequencies (blue color — synchronization mode, yellow — mode of coexistence of synchronous and asynchronous dynamics), *b, e* — order parameter r maps (angular view) and *c, f* (side view). The *a, b, c* maps are obtained for an ensemble of 30 oscillators, and the *d, e, f* maps are obtained for an ensemble of 40 oscillators (color online)

where $\theta_j(t)$ is the instantaneous phase of the j-th oscillator, N is the total number of oscillators, and $\chi(t)$ is the average phase of the oscillators. The time-averaged parameter $r = \langle r(t) \rangle_t$ is also used in the work. The presented maps of the order parameter (see Fig. 1 *(b, c, e, f)*) were calculated separately for each of the 50 initial condition distributions with specified dispersions, and, accordingly, 50 values of the parameter r were calculated for each point on the plane, where different values of the order parameter correspond to different colors. It can be seen from the obtained images (Fig. 1 *(a, d)*) that the mode maps for different ensembles have almost identical regime boundaries. In the synchronization region, the parameter r reaches a value equal to one, which means that there is no phase difference between the oscillators. The differences are seen in Fig. 1 *(c, f)* in the region of the coexistence of synchronous and asynchronous dynamics, where it is seen that the ensembles are characterized by a variety of values of the order parameter r.

For a more visual comparison of regimes with different levels of phase coherence (see Fig. 1 *(b, c, e, f)*) pie charts were constructed showing the percentage of regimes with different values of the order parameter, calculated for all samples of initial conditions with all dispersion values. In Fig. 2 *(a, b)* pie charts for quantifying percentages of various values of the order parameter for ensembles of 30 and 40 oscillators, respectively, are presented. From the diagrams presented, it can be seen that in both cases the most typical value of the order parameter is $r \simeq 1$, which corresponds to the synchronized behavior of the oscillators. In the case of an ensemble of 40 oscillators, where 10 oscillators with zero active and reactive power consumption were added as an intermediate link between the output nodes of generators and consumers, there is a decrease in the percentage of common-mode dynamic regimes. In the considered ensemble, we can observe the appearance of a large variety of values of the order parameter r. So, in the diagram (see Fig. 2 *b*) there is an increase in the percentage of asynchronous regimes with parameter values of the order of $0.49 \leqslant r \leqslant 0.87$.

Now let us look at how the values of the order parameter are distributed in the individual segments of the mode maps shown in Fig. 1 *(b, c)*, that is, when the dispersions of the distributions of the initial values of the instantaneous phase and frequency change in small intervals. Recall that 50 different random samples with specified dispersions were considered. The points $d_\delta = 0.49, d_{\dot\delta} = 0.49$ (region 1) and $d_\delta = 1.835, d_{\dot\delta} = 2.69$ (region 2), were selected, which correspond to the points in the blue and yellow regions of the mode map in Fig. 1, *(a, d)*. From the data shown in Fig. 3 *(a, d)*, it can be seen that at the point $d_\delta = 0.49, d_{\dot\delta} = 0.49$ regardless of the selected ensemble, there is always complete coherence of all oscillators and no phase difference between all oscillators. Thus, region 1 in Fig. 1 *(a, d)* is characterized not only by

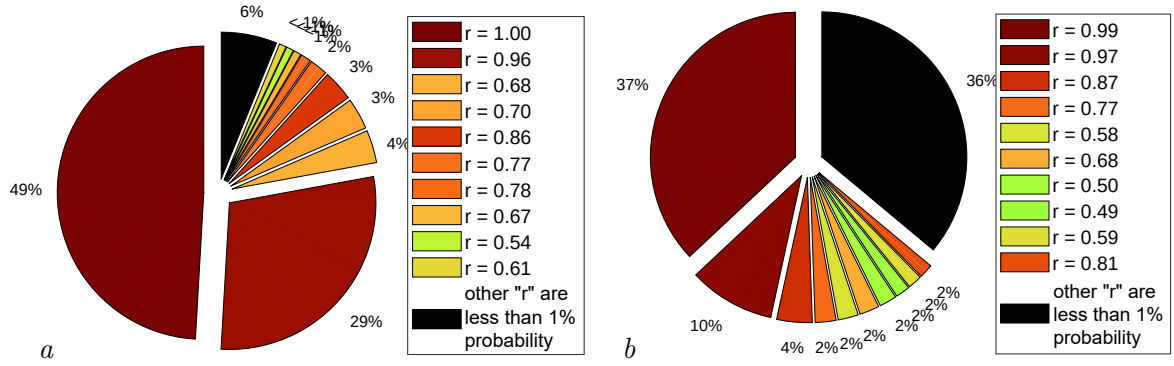

Fig. 2. Distribution of order parameter r values in the form of a pie chart: a — for an ensemble of 30 oscillators, b — for an ensemble of 40 oscillators (color online)

equal instantaneous oscillator frequencies but also by the same instantaneous oscillator phases, and the resulting mode does not depend on the choice of initial conditions. In the coexistence region (Fig. 1 *(a, d)*), multiple dynamic modes can be observed: synchronization of instantaneous frequencies and phases, synchronization of frequencies with constant phase differences, and fully asynchronous behavior. In this case, the number of oscillators considered in the ensemble affects the degree of coherence of the instantaneous phases. This can be seen from Fig. 3 *(b, e)* and Fig. 3 *(c, f)*. It can be seen from the presented figures that for an ensemble of 30 oscillators (Fig. 3 *(b, e)*) the most common mode exhibits near-coherence with an $r = 0.96$ (the probability of observation is 39% for all considered random initial conditions). However, with an increase in the ensemble to 40 oscillators (Fig. 3 *(c, f)*) the closest coherence mode $r = 0.99$ has a probability of about 4%. The most probable values for this ensemble are $r = 0.18$, $r = 0.5$ and $r = 0.87$, for which the probabilities are 18%, 14% and 14% respectively. It is also worth noting the variety of phase dynamics modes in the presented ensemble of oscillators. The obvious disadvantage of the presented value maps of the Kuramoto order parameter r is that they characterize the degree of common-mode oscillators, but do not allow us to identify the area of synchronization of instantaneous frequencies. Only in the case of $r = 1$, when the phases of all oscillators are the same, can it be argued that the instantaneous frequencies of all oscillators coincide. Thus, maps of the order parameter values cannot provide a complete picture of dynamic modes.

2.2. The effect of external noise on the selected dynamic regimes in two ensembles of phase oscillators. Having analyzed the key dynamic modes of the power grid modeled by an ensemble of phase oscillators (1)–(9), and using previously obtained mode maps characterizing the synchronicity of oscillator frequencies (Fig. 1 *(a, d)*) at the points $d_\delta = 0.49, d_{\dot\delta} = 0.49$ and

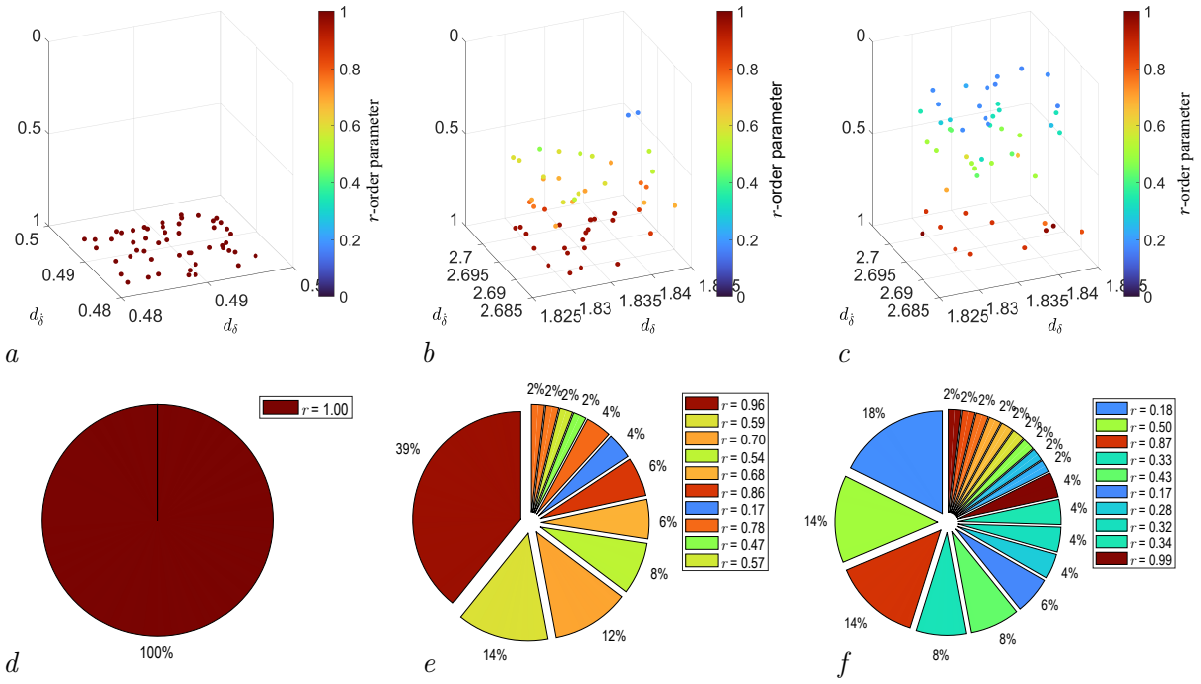

Fig. 3. Maps of the order parameter values plotted for selected segments of the mode maps shown in Fig. 1, *a, d* and the corresponding pie charts of the phase coherence degree (r values): *a, d* — map segment and corresponding pie chart at $d_\delta = 0.49, d_{\dot\delta} = 0.49$ for ensembles of 30 and 40 oscillators, *b, e* — map segment and corresponding pie chart at $d_\delta = 1.835, d_{\dot\delta} = 2.69$ for ensembles of 30 oscillators, *c, f* — map segment and corresponding pie chart at $d_\delta = 1.835, d_{\dot\delta} = 2.69$ for ensembles of 40 oscillators (color online)

$d_\delta = 1.835, d_{\hat{\delta}} = 2.69$, we investigate the effect of Gaussian noise and Levy noise on the obtained network modes. Levy noise is understood as white non-Gaussian noise, which is a derivative of the Levy process (a process with independent non-Gaussian increments) in time. The difference between Gaussian noise and Levy noise lies in the different form of the probability density function. The probability density of Levy noise is characterized by three parameters: α, β and μ. The stability parameter $\alpha \in (0, 2]$ is responsible for the presence of large outliers (it affects the tails of the probability density curve). The parameter $\beta \in [-1, 1]$ characterizes the skewness of the distribution. The parameter μ defines the probability density shift. For distributions that have an average value (that is, for $1 \leqslant \alpha \leqslant 2$), the parameter μ is the average value. For three values of the parameter α, there is an explicit form for probability density functions: for $\alpha = 2$, the probability density is Gaussian (or normal); for $\alpha = 1$, there is a Cauchy distribution, and for $\alpha = 1/2$, there is a Levy distribution. In the case of Levy noise ($\alpha < 2$), the probability density tails are heavier compared to the Gaussian distribution.

Let us consider the frequency and phase synchronization mode of the oscillators at the point $d_\delta = 0.49, d_{\hat{\delta}} = 0.49$ and apply an external noise effect in the form of Gaussian noise and Levy noise to each oscillator of the ensemble. The noise sources in the oscillators are independent. The numerical experiment shows that the studied region is resistant to extremely high intensity values of both Gaussian and Levy noise. As an example, we will demonstrate spatio-temporal diagrams of an ensemble of 40 oscillators exposed to Levy noise with noise parameter values $\alpha = 1$, $\beta = 0$, $\mu = 0$ and intensity $\sigma = 1$. In Fig. 4 *(a, b)* the spatio-temporal diagrams of the instantaneous phases and frequencies of an ensemble of 40 oscillators under the influence of Levy noise are presented. For clarity, the first 100 units of the dimensionless time of the established regime were demonstrated. It can be seen from the spatio-temporal diagram of the instantaneous phases that at the initial moment of time all the instantaneous phases of the oscillators were equal to each other. This is confirmed by Fig. 4 *c*, where the instantaneous value of the Kuramoto order parameter r_{inst} at the initial moment is $r_{\text{inst}} = 1$, while the time-averaged value of $\langle r_{\text{inst}} \rangle_t = 0.19$. The spatio-temporal diagram of instantaneous frequencies demonstrates extreme spikes in the amplitudes of instantaneous frequencies caused by Levy noise. Despite such effects, the oscillators maintain frequency synchronization despite noise, with instantaneous frequencies returning to baseline values. Thus, frequency synchronization is observed in an ensemble of oscillators under the influence of Levy noise, while the phase difference between the oscillators continuously changes under the influence of noise. In the case of exposure to high-intensity Gaussian noise

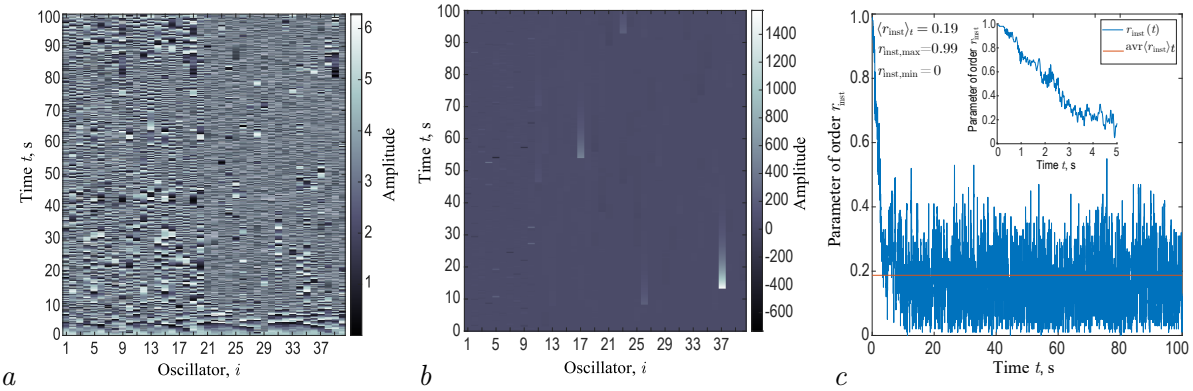

Fig. 4. External influence of Levy noise on an ensemble of 40 oscillators: *a* — spatio-temporal phase diagram, *b* — spatio-temporal frequency diagram, *c* — the temporal realization of the Kuramoto order parameter r_{inst} (color online)

$\sigma > 0.1$ a change in the instantaneous phases and frequencies of the oscillator is observed in the ensemble; however, when noise ceases to affect the ensemble, a sharp synchronization of oscillator frequencies is observed. The results obtained for this area were also observed in the case of a long numerical count time $T = 10000$.

Consider the point $d_\delta = 1.835, d_{\dot\delta} = 2.69$, in which a mode of coexistence of synchronous and asynchronous dynamics are observed. Let us select the initial conditions under which asynchronous dynamics is observed in the studied ensembles, that is, at least one of the oscillators rotates with a natural frequency different from the frequency of the oscillators of the cluster. Let us perform a numerical experiment with the effect of Gaussian noise on the studied ensembles of oscillators. The noise sources in the oscillators, as in the previous case, are independent. The numerical result showed that a high degree of resistance to external Gaussian effects is demonstrated in the area of the studied mode of the power grid model. For example, for an ensemble of 30 oscillators, a change in spatio-temporal dynamics was observed at an extreme noise intensity of $\sigma = 0.1833$ (Fig. 5 *(a, b, c)*), whereas for an ensemble of 40 oscillators, this value was observed at $\sigma = 0.2732$ (Fig. 5 *(d, e, f)*). It is also worth noting that changes in the spatio-temporal dynamics of ensembles were observed with a sufficiently long numerical integration time $T = 10000$. For both ensembles, there was a breakdown in the frequency synchronism of oscillators modeling energy consumers (oscillators from $i = 11$ to $i = 30$ or $i = 40$ simulate energy consumers, while the remaining oscillators belong to energy generators in both ensembles considered). The instantaneous frequency of desynchronized oscillators converges to the value of the instantaneous frequency of the oscillator already in asynchronous mode prior to external perturbation.

Next, we will consider the same area of the initial modes, replacing the external effect with Levy noise, and conduct a numerical experiment when changing noise parameters such as α and β. The results obtained are shown in Fig. 6 and Fig. 7. In the diagrams shown in Fig. 6, the

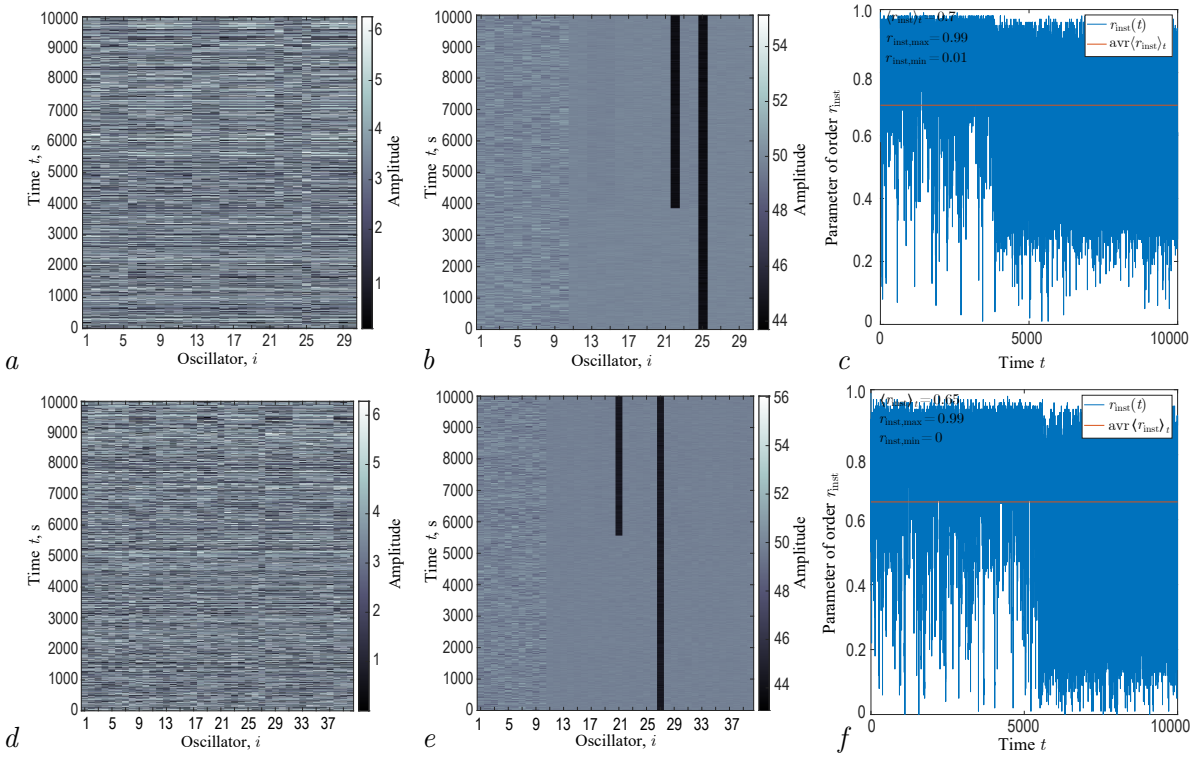

Fig. 5. Gaussian noise effects: *a, d* phase diagrams; *b, e* frequency diagrams; *c, f* Kuramoto order parameter for 30- and 40-oscillator ensembles (color online))

threshold values of Levy noise intensity relative to the parameters α and β are shown, at which a change in the spatio-temporal dynamics of ensembles was observed. Consider the case of the zero value of the skewness parameter ($\beta = 0$). In this case, at $\alpha = 1$, the threshold noise intensity in the studied ensembles of 30 and 40 oscillators has the values $\sigma = 2.84 \cdot 10^{-6}$ and $\sigma = 2.2 \cdot 10^{-6}$ respectively. Further, with an increase in the parameter α, the threshold values of Levy noise monotonously increase, and with a value of $\alpha = 1.9$, a sharp jump in the threshold noise intensity occurs for both cases of ensembles. The observed behavior of noise intensity thresholds is related

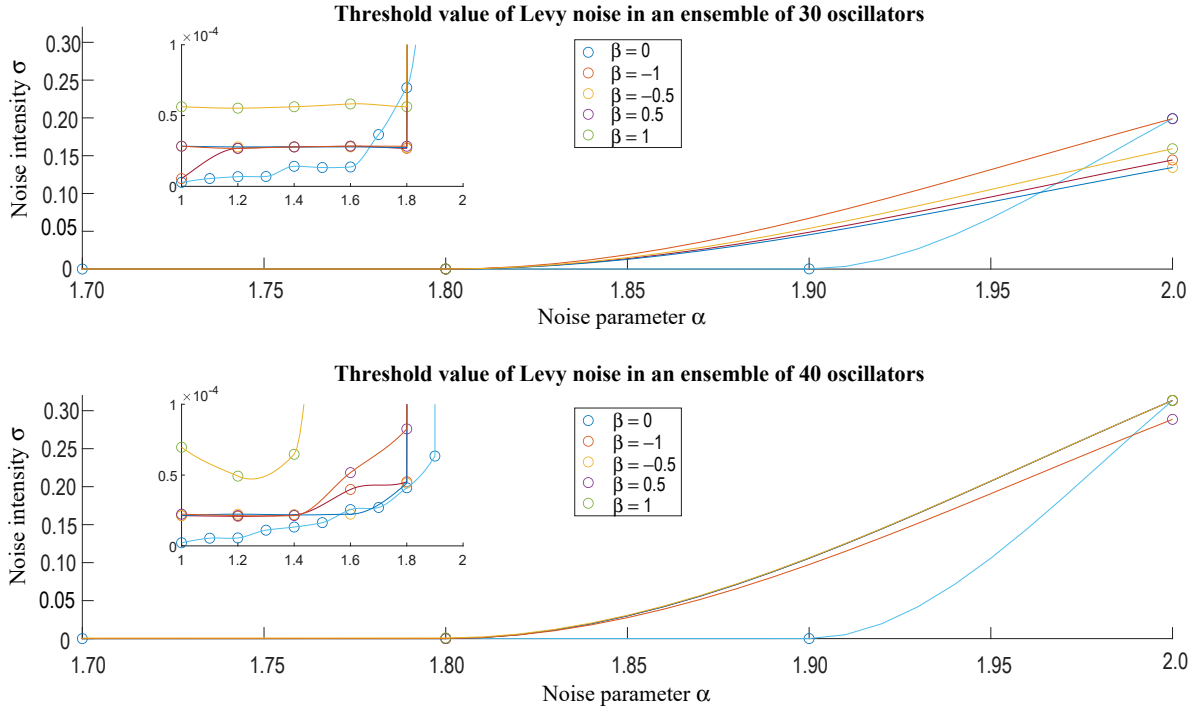

Fig. 6. Levy noise intensity values at which changes in spatio-temporal dynamics in ensembles of 30 and 40 oscillators are observed (color online)

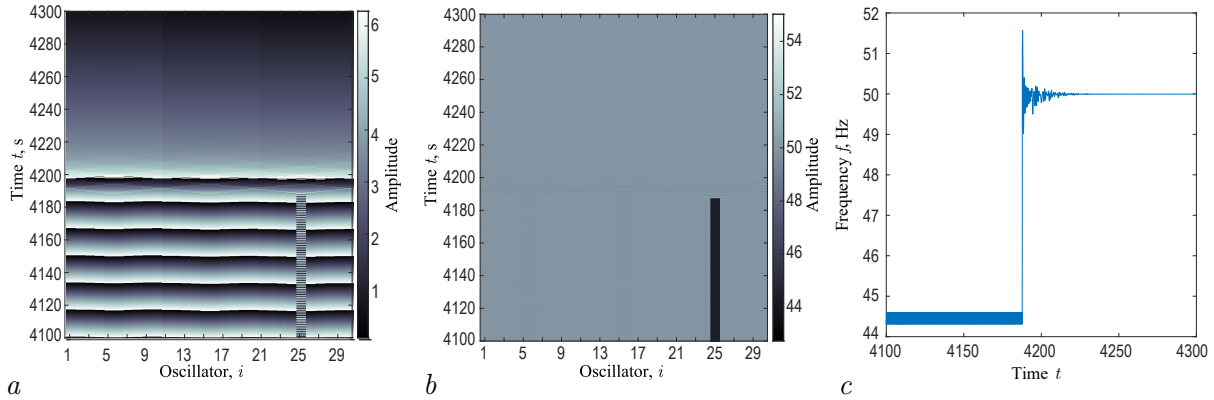

Fig. 7. External influence of Levy noise with parameters $\alpha = 1.4$, $\beta = 0$, $\sigma = 1.42 \cdot 10^{-5}$ on an ensemble of 30 oscillators: *a* — spatio-temporal diagram of instantaneous phases, *b* — spatio-temporal diagram of instantaneous frequencies, *c* — time realization of the instantaneous frequency of the oscillator $i = 25$ (color online)

to the Levy noise feature. When α increases, the probability of sudden impulse bursts decreases, and the frequency of such bursts also decreases, and when the value of $\alpha = 2$ is reached, the high-amplitude effects disappear. Thus, the obtained values of the threshold intensity σ at $\alpha = 2$ are $\sigma = 0.199$ and $\sigma = 0.3135$ for ensembles of 30 and 40 oscillators, respectively. In the presence of an asymmetry in the probability distribution of Levy noise in the range $-1 \leqslant \beta \leqslant 0.5$ there is a slight increase in the threshold intensity for the parameter $1 \leqslant \alpha \leqslant 1.8$ for both studied oscillator ensembles. For the parameter $\beta = 1$ in the range $1 \leqslant \alpha \leqslant 1.8$, the threshold intensity is highest for $\beta = 1$; however, as α approaches 2, the threshold intensities are close to the value obtained at $\beta = 0$. This means that the presence of non-zero asymmetry in Levy noise has an effect only if there are sharp high-amplitude random noise values. So, in Fig. 6 it can be seen that the considered oscillator ensembles are less sensitive to Levy noise at $\beta = 0.5$ and $\beta = 1$. This suggests that oscillators in ensembles are more resistant to sudden increases in instantaneous frequency due to high-amplitude random effects.

In the considered area of the coexistence of synchronous and asynchronous dynamics, the phenomenon of oscillator synchronization under the influence of Levy noise was observed. As an example, in Fig. 7 illustrates the phenomenon in which a high-amplitude pulse effect of Levy noise synchronizes an oscillator that is in asynchronous mode at the initial moment of integration time. As can be seen from Fig. 7, *c*, at time $T \approx 4195$ there is a sharp jump in the instantaneous frequency towards an increase in the oscillation frequency, followed by the establishment of the instantaneous frequency near the reference value of ω_R (Table 1). It is also worth noting that after frequency synchronization is established, phase coherence of the oscillators is also observed in the ensemble; the time-averaged order parameter approaches $r_{\text{inst}} \approx 1$.

Conclusion

This study investigates a power grid with a ring-shaped topology, which was represented as two independent ensembles of 30 and 40 elements, respectively. The network elements represent generators and consumers of energy and are described by first- and second-order phase oscillators [24]. Ensembles of 40 oscillators are distinguished by the presence of consumers with zero active and reactive power. To compare the spatio-temporal dynamics of two different ensembles, mode maps for the frequency and phase dynamics of the ensembles were constructed. The mode maps were obtained with unchangeable control parameters of the model and variable random initial conditions, which are set using a normal distribution with different values of variance of random variables. The dispersion for initial phases and frequencies was varied independently, and the mode maps themselves were constructed with 50 random samples of initial conditions.

The mode maps obtained in this way demonstrated a wide variety of spatio-temporal modes without changing any control parameters. For example, the mode maps obtained as a result of the instantaneous frequency analysis is identical for the two ensembles considered and contains areas of synchronization, complete synchronization of phases and frequencies of oscillators, and asynchronous mode. The area of complete synchronization under all the considered initial conditions was observed at small values of the dispersion of the initial phases of the oscillators, whereas all of the above modes were observed with an increase in the dispersion of the initial phases. The resulting area on the mode map was designated as the area of coexistence of synchronous and asynchronous dynamics, where the appearance of a particular mode was determined by a set of random variables.

Maps of the order parameter values were constructed to assess the degree of phase coherence in the ensemble. The magnitude of phase coherence is a Kuramoto order parameter r averaged

over the simulation time. The mode maps obtained in this way for the studied ensembles showed varying degrees of coherence. Thus, the greatest variety of levels of phase coherence was observed in an ensemble of 40 oscillators. This is due to the presence of oscillators in the ensemble that simulate consumers with zero active power, whose natural frequencies [24] are different from generators and other consumers in the power grid. Such a variety of natural frequency values complicates the establishment of complete phase coherence in the ensemble and contributes to the emergence of new levels of phase coherence. However, in the area of complete synchronization, complete phase coherence $r = 1$ was observed under any initial conditions, regardless of the ensemble under study.

A study with noise influences of various types, such as Gaussian noise and Levy noise, was conducted in two areas of the mode map, demonstrating the frequency synchronization of oscillators. The area of the mode map in which exceptionally complete synchronization existed demonstrated strong resistance to Gaussian and Levy noise, regardless of the noise intensity values, including extreme values. The observed stability in the studied mode consisted in the establishment of frequency synchronization of the ensemble after the cessation of noise exposure, while the phase difference between the oscillators became non-zero; that is, complete synchronization in the ensemble after exposure to various types of noise was not observed. If noise affects the area of coexistence of synchronous and asynchronous dynamics, switching between synchronization and asynchronous behavior of ensembles is possible under the influence of Gaussian noise and Levy noise. In the case of Gaussian noise, mode switching was observed at extreme values of noise intensity, whereas in the case of Levy noise, the required noise intensity for mode change depended on the parameter α. So, with the parameter $\alpha = 1$ the Levy noise intensity could be 10^{-6}, and with $\alpha = 2$, no more than 0.5. Such different threshold noise intensities in the case of Gaussian exposure and Levy noise are related to the Levy noise feature, which is characterized by high-amplitude random bursts. With decreasing parameter α, the probability of such outliers increases. The effect of the Levy noise asymmetry parameter β slightly changes the noise intensity thresholds and only at $\beta = 1$ does the threshold intensity increase. The results obtained in the study area of the coexistence of various synchronous and asynchronous modes indicate that the studied ensembles of phase oscillators are more sensitive to pulsed external influences than to conventional noise.

The numerical results of the model under study can be of practical importance in determining the conditions of stable operation of real power systems. In particular, the influence of noise effects can have practical application in the development of mechanisms to counteract internal and external disturbances exerted on the power grid. The results obtained when Gaussian noise and Levy noise are applied to the power grid indicate that power grids can be quite resistant to ordinary, normally distributed noise and are highly vulnerable to impulsive disturbances and sudden disturbances, which corresponds to Lévy noise with $\alpha < 2$. Thus, in real power grids, special attention should be paid to pulsed disturbances in order to maintain stable network operation.

References

1. Ackermann T, Andersson G, Söder L. Distributed generation: a definition. Electric Power Systems Research. 2001;57(3):195–204. DOI: 10.1016/S0378-7796(01)00101-8.
2. Milan P, Wächter M, Peinke J. Turbulent character of wind energy. Phys. Rev. Lett. 2013;110(13):138701. DOI: 10.1103/PhysRevLett.110.138701.
3. Heide D, von Bremen L, Greiner M, Hoffmann C, Speckmann M, Bofinger S. Seasonal optimal mix of wind and solar power in a future, highly renewable Europe. Renewable Energy. 2010;35(11):2483–2489. DOI: 10.1016/j.renene.2010.03.012.

4. Heide D, Greiner M, von Bremen L, Hoffmann C. Reduced storage and balancing needs in a fully renewable European power system with excess wind and solar power generation. Renewable Energy. 2011;36(9):2515–2523. DOI: 10.1016/j.renene.2011.02.009.
5. Anvari M, Lohmann G, Wächter M, Milan P, Lorenz E, Heinemann D, Tabar MRR, Peinke J. Short term fluctuations of wind and solar power systems. New J. Phys. 2016;18(6): 063027. DOI: 10.1088/1367-2630/18/6/063027.
6. Anvari M, Wächter M, Peinke J. Phase locking of wind turbines leads to intermittent power production. Europhysics Letters. 2017;116(6):60009. DOI: 10.1209/0295-5075/116/60009.
7. Schmietendorf K, Peinke J, Kamps O. The impact of turbulent renewable energy production on power grid stability and quality. Eur. Phys. J. B. 2017;90:222. DOI: 10.1140/epjb/e2017-80352-8.
8. Schäfer B, Beck C, Aihara K, Witthaut D, Timme M. Non-Gaussian power grid frequency fluctuations characterized by Lévy-stable laws and superstatistics. Nat. Energy. 2018;3(2): 119–126. DOI: 10.1038/s41560-017-0058-z.
9. Lee D, Chiang Y, Chen YT, Tsai HH. Impacts of battery energy storage system on power grid smartness: Case study of Taiwan Power Company. Journal of Energy Storage. 2024;86:111188. DOI: 10.1016/j.est.2024.111188.
10. Dorfler F, Bullo F. Synchronization and transient stability in power networks and nonuniform Kuramoto oscillators. SIAM Journal on Control and Optimization. 2012;50(3):1616–1642. DOI: 10.1137/110851584.
11. Arenas A, Díaz-Guilera A, Kurths J, Moreno Y, Zhou C. Synchronization in complex networks. Physics Reports. 2008;469(3):93–153. DOI: 10.1016/j.physrep.2008.09.002.
12. Filatrella G, Nielsen AH, Pedersen NF. Analysis of a power grid using a Kuramoto-like model. Eur. Phys. J. B. 2008;61:485–491. DOI: 10.1140/epjb/e2008-00098-8.
13. Choi YP, Ha SY, Yun SB. Complete synchronization of Kuramoto oscillators with finite inertia. Physica D. 2011;240(1):32–44. DOI: 10.1016/j.physd.2010.08.004.
14. Lozano S, Buzna L, Díaz-Guilera A. Role of network topology in the synchronization of power systems. Eur. Phys. J. B. 2012;85:231. DOI: 10.1140/epjb/e2012-30209-9.
15. Fortuna L, Frasca M, Sarra Fiore A. A network of oscillators emulating the Italian high-voltage power grid. International Journal of Modern Physics B. 2012;26(25):1246011. DOI: 10.1142/S0217979212460113.
16. Rohden M, Sorge A, Timme M, Witthaut D. Self-organized synchronization in decentralized power grids. Phys. Rev. Lett. 2012;109(6):064101. DOI: 10.1103/PhysRevLett.109.064101.
17. Carareto R, Baptista MS, Grebogi C. Natural synchronization in power-grids with anti-correlated units. Communications in Nonlinear Science and Numerical Simulation. 2013; 18(4):1035–1046. DOI: 10.1016/j.cnsns.2012.08.030.
18. Motter AE, Myers SA, Anghel M, Nishikawa T. Spontaneous synchrony in power-grid networks. Nature Phys. 2013;9(3):191–197. DOI: 10.1038/nphys2535.
19. Dörfler F, Bullo F. Synchronization in complex networks of phase oscillators: A survey. Automatica. 2014;50(6):1539–1564. DOI: 10.1016/j.automatica.2014.04.012.
20. Olmi S, Navas A, Boccaletti S, Torcini A. Hysteretic transitions in the Kuramoto model with inertia. Phys. Rev. E. 2014;90(4):042905. DOI: 10.1103/PhysRevE.90.042905.
21. Grzybowski JMV, Macau EEN, Yoneyama T. On synchronization in power-grids modelled as networks of second-order Kuramoto oscillators. Chaos. 2016;26(11):113113. DOI: 10.1063/1.4967850.
22. Mirollo RE, Strogatz SH. The spectrum of the locked state for the Kuramoto model of coupled oscillators. Physica D. 2005;205(1–4):249–266. DOI: 10.1016/j.physd.2005.01.017.
23. Delabays R, Coletta T, Jacquod P. Multistability of phase-locking in equal-frequency Kuramoto models on planar graphs. J. Math. Phys. 2017;58(3):032703. DOI: 10.1063/

1.4978697.
24. Nishikawa T, Motter AE. Comparative analysis of existing models for power-grid synchroni zation. New J. Phys. 2015;17(1):015012. DOI: 10.1088/1367-2630/17/1/015012.
25. Manik D, Witthaut D, Schäfer B, Matthiae M, Sorge A, Rohden M, Katifori E, Timme M. Supply networks: Instabilities without overload. Eur. Phys. J. Spec. Top. 2014;223:2527–2547. DOI: 10.1140/epjst/e2014-02274-y.
26. Coletta T, Jacquod P. Linear stability and the Braess paradox in coupled-oscillator networks and electric power grids. Phys. Rev. E. 2016;93(3):032222. DOI: 10.1103/PhysRevE.93.032222.
27. Machowski J, Lubosny Z, Bialek JW, Bumby JR. Power System Dynamics: Stability and Control. N.Y.: Wiley; 2020. 896 p.
28. Tumash L, Olmi S, Schöll E. Stability and control of power grids with diluted network topology. Chaos. 2019;29(12):123105. DOI: 10.1063/1.5111686.
29. Gotz M, Rapp M, Dostert K. Power line channel characteristics and their effect on communication system design. IEEE Communications Magazine. 2004;42(4):78–86. DOI: 10.1109/MCOM.2004.1284933.
30. González-Ramos J, Uribe-Pérez N, Sendin A, Gil D, de la Vega D, Fernández I, Núñez IJ. Upgrading the power grid functionalities with broadband power line communications: Basis, applications, current trends and challenges. Sensors. 2022;22(12):4348. DOI: 10.3390/s22124348.
31. Bai T, Zhang H, Wang J, Xu C, Elkashlan M, Nallanathan A, Hanzo L. Fifty years of noise modeling and mitigation in power-line communications. IEEE Communications Surveys & Tutorials. 2020;23(1):41–69. DOI: 10.1109/comst.2020.3033748.
32. Antoniali M, Versolatto F, Tonello AM. An experimental characterization of the PLC noise at the source. IEEE Transactions on Power Delivery. 2015;31(3):1068–1075. DOI: 10.1109/TPWRD.2015.2452939.
33. Di Bert L, Caldera P, Schwingshackl D, Tonello AM. On noise modeling for power line communications. In: IEEE International Symposium on Power Line Communications and Its Applications. 2011, Udine, Italy. IEEE; 2011. P. 283–288. DOI: 10.1109/ISPLC.2011.5764408.
34. Meng H, Guan YL, Chen S. Modeling and analysis of noise effects on broadband power-line communications. IEEE Transactions on Power Delivery. 2005;20(2):630–637. DOI: 10.1109/TPWRD.2005.844349.
35. Nassar M, Gulati K, Mortazavi Y, Evans BL. Statistical modeling of asynchronous impulsive noise in powerline communication networks. In: 2011 IEEE Global Telecommunications Conference-GLOBECOM 2011. 2011, Houston, TX, USA. IEEE; 2011. P. 1–6. DOI: 10.1109/GLOCOM.2011.6134477.
36. Ferreira HC, Lampe L, Newbury J, Swart TG. Power Line Communications: Theory and Applications for Narrowband and Broadband Communications over Power Lines. N.Y.: Wiley; 2010. 536 p.
37. Nassar M, Dabak A, Kim IH, Pande T, Evans BL. Cyclostationary noise modeling in narrowband powerline communication for smart grid applications. In: IEEE International Conference on Acoustics, Speech and Signal Processing (ICASSP). 2012, Kyoto, Japan. IEEE; 2012. P. 3089–3092. DOI: 10.1109/ICASSP.2012.6288568.
38. Zimmermann M, Dostert K. Analysis and modeling of impulsive noise in broad-band powerline communications. IEEE Transactions on Electromagnetic Compatibility. 2002;44(1):249–258. DOI: 10.1109/15.990732.
39. Klatt M, Meyer J, Schegner P, Koch A, Myrzik J, Darda T, Eberl G. Emission levels above 2 kHz-Laboratory results and survey measurements in public low voltage grids. In: 22nd

International Conference and Exhibition on Electricity Distribution (CIRED 2013). 2013, Stockholm, Sweden. IEEE; 2013. P. 1–4. DOI: 10.1049/cp.2013.1102.
40. Fernandez I, Uribe-Pérez N, Eizmendi I, Angulo I, de la Vega D, Arrinda A, Arzuaga T. Characterization of non-intentional emissions from distributed energy resources up to 500 kHz: A case study in Spain. International Journal of Electrical Power & Energy Systems. 2019;105:549–563. DOI: 10.1016/j.ijepes.2018.08.048.
41. Yalcin T, Özdemir M, Kostyla P, Leonowicz Z. Analysis of supra-harmonics in smart grids. In: IEEE International Conference on Environment and Electrical Engineering and 2017 IEEE Industrial and Commercial Power Systems Europe (EEEIC/I&CPS Europe). 2017, Milan, Italy. IEEE; 2017. P. 1–4. DOI: 10.1109/EEEIC.2017.7977812.
42. Bollen M, Olofsson M, Larsson A, Rönnberg S, Lundmark M. Standards for supraharmonics (2 to 150 kHz). IEEE Electromagnetic Compatibility Magazine. 2014;3(1):114–119. DOI: 10.1109/MEMC.2014.6798813.
43. Larsson EA, Bollen MH, Wahlberg MG, Lundmark CM, Rönnberg SK. Measurements of high-frequency (2–150 kHz) distortion in low-voltage networks. IEEE Transactions on Power Delivery. 2010;25(3):1749–1757. DOI: 10.1109/TPWRD.2010.2041371.
44. Larsson EOA, Bollen MHJ. Measurement result from 1 to 48 fluorescent lamps in the frequency range 2 to 150 kHz. In: Proceedings of 14th International Conference on Harmonics and Quality of Power-ICHQP 2010. 2010, Bergamo, Italy. IEEE; 2010. P. 1–8. DOI: 10.1109/ICHQP.2010.5625395.
45. Rönnberg SK, Bollen MH. Emission from four types of LED lamps at frequencies up to 150 kHz. In: IEEE 15th International Conference on Harmonics and Quality of Power. 2012, Hong Kong, China. IEEE; 2012. P. 451–456. DOI: 10.1109/ICHQP.2012.6381216.
46. Zimmerman R, Murillo-Sanchez C, Thomas R. MATPOWER: Steady-State Operations, Planning, and Analysis Tools for Power Systems Research and Education. IEEE Transactions on Power Systems. 2011;26(1):12–19. DOI: 10.1109/TPWRS.2010.2051168.
47. Cañizares C, Fernandes T, Geraldi Jr E., Gerin-Lajoie L, Gibbard M, Hiskens I, Kersulis J, Kuiava R, Lima L, De Marco F, Martins N, Pal BC, Piardi A, Ramos R, dos Santos J, Silva D, Singh AK, Tamimi B, Vowles D. IEEE PES Technical Report TR-18: Benchmark Systems for Small-Signal Stability Analysis and Control. IEEE PES Resource Center; 2015. 390 p.
48. Kuramoto Y. Self-entrainment of a population of coupled non-linear oscillators. In: Araki H, editor International Symposium on Mathematical Problems in Theoretical Physics. Lecture Notes in Physics. Vol. 39. Berlin: Springer; 1975. P. 420–422. DOI: 10.1007/BFb0013365.